Adaptive Field-to-Mask Procedure for the Synthesis of Metalens Antennas with Complex Near Field Coverage Patterns in 5G Scenarios

Álvaro F. Vaquero, *Member, IEEE*, Marcos R. Pino, and Manuel Arrebola, *Senior Member, IEEE*

***Abstract*— This work presents a novel procedure to address the synthesis of metalens antennas with tight requirements in near-field complex scenarios. A model to compute the near field is introduced together with the Intersection Approach algorithm (IA) for metalens antennas, for the first time. Then, the adaptive field-to-mask (F2M) procedure is introduced. The F2M is applied in the definition of the templates of local optimization algorithms, enhancing their convergence. F2M progressively defines the templates as intermediate solutions between the starting point and the specifications considering the radiated field behavior in each intermediate stage. The advantages of F2M are demonstrated with two examples which synthesizes the amplitude of the near field in a challenging scenario, setting constraints in a transverse and offset plane to the metalens aperture. One of the syntheses aims to reach a uniform field distribution through a curved corridor in a range of 14 m to provide coverage at 39 GHz. The synthesized phase-shift distribution is used to design and manufacture a prototype to evaluate its performance. The measurements agree with both synthesis and full-wave results. Optimization algorithms, such as IA, can take an advantage of the F2M procedure to reach hard patterns in near-field complex scenarios.**

***Index Terms*—Near-field synthesis, metalens antennas, near-field pattern, near field coverage.**

I. Introduction

WIRELESS TECHNOLOGY provides attractive features for some applications, such as Radio Frequency Identification (RFID) [1], Wireless Power Transfer (WPT) [2], and measurement systems [3], among others throughout the last years. The latest developments in communication systems, in particular the evolution of the current Fifth Generation (5G) of mobile communications has boosted the interest in wireless technology to its peak. The new generation of mobile communications, 5G, beyond 5G (B5G), or even the future 6G, has advanced the use of higher frequencies, looking for larger bandwidths and higher data-rate communications. In this line, the sub-6 band, or Frequency Range 1 (FR1) [4] gathers the communication systems deployed within frequencies lower than 6 GHz. However, a major research challenge is found in future communication systems deployed in the mm-wave frequency band. These systems are planned to operate in different bands from 28 to 200 GHz to obtain high-speed wireless access in cellular networks [5], [6]. A major issue to deploy communication systems in K_a-band or higher frequencies is related to signal propagation. Particularly, the path losses and the sensitivity to physical barriers notably increase at those frequencies compared to FR1 [7], [8]. Both issues can be reduced by a proper design of the base station antennas.

Antennas are a key subsystem that must be adapted to the requirements imposed by the new wireless applications and technologies as well as the scenarios where they will be deployed. This means providing efficient coverage and radio links and, from the point of view of the devices, wireless connectivity through a suitable and proper antenna design. In indoor scenarios the distance between users and base stations is much shorter than in outdoor placements, and the devices will be placed within the radiative near field of the base station, the Fresnel zone. Hence, the deployment of efficient indoor communication systems working within the radiative near field will be mandatory or, even a desired option to enhance 5G and beyond communications. Although massive MIMO is the preferable solution for 5G [9], [10], the complexity of indoor scenarios requires analyzing and providing other solutions. These indoor scenarios imply forgetting extensive coverage areas provided by an outer base station in support of small areas wherein the devices are found. In addition, indoor base stations can cover areas that are not linked to outer base stations due to "blind" or "dead" zones (areas with poor or even null coverage) [11]-[14]. Thus, developing antennas with near-field-shaped beams, like far-field patterns, will be a key factor in current and future communication systems.

A suitable candidate for acting as an indoor base station is a spatially fed array (SFA) antenna. These antennas are defined as a combination of a primary feed and a phased array antenna, such as reflectarray, metalens or metasurface antennas. The use of a primary feed removes the need for a feeding network to excite the elements. Therefore, the radiation efficiency is

This work was supported in part by the Ministerio de Ciencia e Innovación and Agencia Española de Investigación within the Project ENHANCE-5G (PID2020-114172RB-C21/AEI/10.13039/501100011033).

The authors are with the Department of Electrical Engineering, Group of Signal Theory and Communications, Universidad de Oviedo, 33203, Gijón, Spain (e-mail: fernandezvalvaro@uniovi.es, mpino@uniovi.es, arrebola@uniovi.es).

improved compared with an array antenna, especially at mm-wave or higher bands. This solution obtains an efficiency close to that of conventional reflectors [15]. Other two important advantages are given by SFA antennas. First, an SFA is a compact low-cost solution that is easily integrated with indoor scenarios. Second, a range of different published works has demonstrated that SFA antennas can reach complex shaped patterns with severely tight requirements for space communications [16]-[18]. However, most of these published works are related to the synthesis of the far-field radiated by an SFA. Only a few recent examples are found for the synthesis of the near-field components of SFA [19], [20]. The first one is based on a multi-focus approach, while [20] uses an iterative application of the direct and inverse FFT. Although these approaches present successful results, both are limited in the geometries addressed since the use of the FFT limits the application of templates to planes parallel to the antenna aperture and the multi-foci approach to patterns like focused beams. A general approach to address complex shaped patterns within the near field of a reflectarray is presented in [21], which is based on the generalized Intersection Approach (gIA) for the near-field. The gIA together with the finite difference technique [22] provides a very efficient approach to reaching complex shaped-beam patterns in arbitrary configurations within the radiated near-field.

A common approach to deal with these optimizations is to divide the process into different synthesis subprocesses (or stages). In each subprocess the specifications are tightened, and the starting point is also improved [23]-[25]. Owing to the IA is a local search algorithm [26], an improved starting point closer to the desired solution would enhance the convergence. An important weakness of these strategies concerns the strong dependence on both, starting points and specifications. Thus, a proper selection of the starting point, as well as a definition of the mask, is a major issue in the synthesis process. Most of these strategies are applied for far-field synthesis, though a few examples may be found for near field.

In this work, the IA is presented for synthesizing a metalens antenna with constraints in the magnitude of the near field to radiate a uniform-field distribution in a complex scenario. Besides, a novel strategy to address complex scenario requirements is presented. This work aims to generate a complex near-field coverage area, which is defined in a plane transverse and offset to the antenna aperture through several meters. This type of scenario implies considering different effects on the definitions of the templates, such as the strong difference in the relative level of the electric field due to the propagation. The proposed procedure used itself electric field to define the templates giving intermediate solutions that ease the convergence of the gIA. Besides, the proposed method overcomes the definition of carrying out the synthesis process by imposing conditions in planes parallel to the antenna aperture. The procedure shows successful results in these quite challenging scenarios, resulting in a phase-shift distribution that radiates a suitable shaped near-field pattern. Then, the proposed procedure is demonstrated by designing and manufacturing a prototype that is evaluated in a planar acquisition range. The experimental validation presents a high agreement with both synthesis and full-wave results.

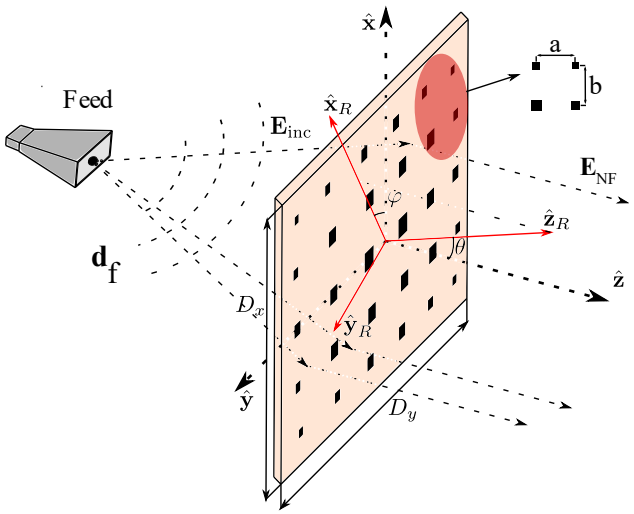

Fig. 1. Sketch of a centered-optic printed transmit-array.

II. Metalens Design: Analysis and Synthesis

In this section, a description of the gIA for metalens antennas in near field is provided. Before further explaining the gIA, a model to compute the radiated near field of a metalens is presented.

A. Radiated near-field

Fig. 1 shows the scheme of the metalens optics. The metalens is comprised of a primary feed, which typically is a horn antenna, and an arrangement of radiating elements (printed, dielectric- or metal-only elements). A linearly polarized primary feed illuminates the surface of the metalens providing an incident field $\boldsymbol{E}_{inc}$. The elements of the metalens are phase shifters that introduce a certain delay and loss in the incident field, resulting in the following tangential transmitted field,

$$\boldsymbol{E}_{tr}^{X/Y}(x_l, y_l) = E_{tr,x}^{X/Y}(x_l, y_l)\hat{x} + E_{tr,y}^{X/Y}(x_l, y_l)\hat{y} \tag{1}$$

where the superscripts denote the polarization of the feed and the subscript the field component projected onto the array surface. The (x_l, y_l) coordinates represent the location of the lth element, taking the center of the metalens as the center of coordinates (see Fig. 1).

The relation between $\boldsymbol{E}_{inc}$ and $\boldsymbol{E}_{tr}$ is defined by

$$\boldsymbol{E}_{tr}^{X/Y}(x_l, y_l) = \overline{\boldsymbol{T}}^l \cdot \boldsymbol{E}_{inc}^{X/Y}(x_l, y_l) \tag{2}$$

where $\overline{\boldsymbol{T}}^l$ is the transmission matrix and fully characterizes the electromagnetic behavior of the lth element

$$\overline{\boldsymbol{T}}^l = \begin{pmatrix} \tau_{xx}^l & \tau_{xy}^l \\ \tau_{yx}^l & \tau_{yy}^l \end{pmatrix} \tag{3}$$

The elements of $\overline{\boldsymbol{T}}^{l}$ are complex numbers that characterize the amplitude and phase of the transmission performance introduced by each element of the metalens. For achiral cells, τ_{xx} and τ_{yy} are the direct coefficients, which mainly control the copolar component of the radiated field in linear polarization, while τ_{xy} and τ_{yx} are the cross coefficients, with contribution in the cross-polar. From now on, the copolar component of the radiated near field should be understood as the main component of the field associated with the copolar of the feeder, while the crosspolar will be the orthogonal component considering linear polarization.

The near field is computed by means of Huygens' Principle and the Principle of Superposition. The aperture of the metalens is divided into several subdomains, which are considered small radiating apertures, hereinafter subapertures. Then, the near field radiated by the whole metalens on the observation point $\boldsymbol{r}$ is the contribution of each subdomain on $\boldsymbol{r}$. Therefore, the near field can be expressed as

$$\boldsymbol{E}_{NF}(\boldsymbol{r}) = \sum_{i=1}^{N_{xy}} \boldsymbol{E}_{NF,i}(\boldsymbol{r}) \tag{4}$$

where N_{xy} is the number of subdomains in which the aperture is divided, and $\boldsymbol{E}_{NF,i}$ is the radiation of the i-th radiating subaperture (subdomain) on the observation point $\boldsymbol{r}$.

The contribution of the whole radiating aperture (metalens) can be computed using the classical theory of planar aperture distributions for near-field patterns [28]. However, if the observation point $\boldsymbol{r}$ is in the Fraunhofer region of the subaperture, the contribution of the subaperture can be computed under far-field assumption [28]. Note that $\boldsymbol{r}$ is beyond the Fraunhofer distance of the subaperture but within the Fresnel zone of the whole metalens. This consideration simplifies the formulation at the cost of establishing a minimum distance to compute the near field. If each subaperture is identified as an element of the metalens, the minimum distance is given by

$$\boldsymbol{r}_{min} = \frac{2(a^2+b^2)}{\lambda_0} + \lambda_0 \tag{5}$$

where a and b are the dimensions of the subaperture (size of the metalens cell), and λ_0 the wavelength in vacuum.

This assumption does not present a strong limitation in the model since most of the applications require to compute the near field in a point $\boldsymbol{r} \gg \boldsymbol{r}_{min}$. Now, (4) can be written as

$$\boldsymbol{E}_{NF}(\boldsymbol{r}) = \sum_{i=1}^{N_{xy}} \boldsymbol{E}_{FF,i}(\boldsymbol{r}) \tag{6}$$

where $\boldsymbol{E}_{FF,i}$ is the far-field radiated by the i-th subaperture on $\boldsymbol{r}$. The position vector of the observation point considering the origin of the coordinate system at the center of the i-th subaperture is obtained as

$$\boldsymbol{r_i} = \boldsymbol{r} - \boldsymbol{r_{ap,i}} = r_i\, \hat{\boldsymbol{r}}_{\boldsymbol{i}} \tag{7}$$

where $\boldsymbol{r_{ap,i}}$ is the position vector of the i-th subaperture and r_i is the distance between the observation point and the center of the radiating subaperture. Thus, the contribution of each one can be written in terms of the propagation from the subaperture to the observation point and the active element pattern $\boldsymbol{F}(\theta_i, \varphi_i)$, in the direction of the observation point (θ_i, φ_i).

$$\boldsymbol{E}_{FF,i}(\boldsymbol{r}) = \frac{jk}{4\pi}\frac{e^{-jkr_i}}{r_i}\boldsymbol{F}(\theta_i, \varphi_i) \tag{8}$$

Finally, the contribution can be computed by means of the Love's Principle of Equivalence [28], and it can be expressed as in terms of it θ_i- and φ_i-component as

$$\boldsymbol{E}_{FF,i}(\boldsymbol{r}) = \frac{jk}{4\pi}\frac{e^{-jkr_i}}{r_i}\left[E_{\theta_i}\,\widehat{\boldsymbol{\theta}}_{\boldsymbol{i}} + E_{\varphi_i}\widehat{\boldsymbol{\varphi}}_{\boldsymbol{i}}\right] \tag{9.a}$$

$$E_{\theta_i} = P_{x_i}\cos\varphi_i + P_{y_i}\sin\varphi_i - \eta\cos\theta_i\left(Q_{x_i}\sin\varphi_i - Q_{y_i}\cos\varphi_i\right) \tag{9.b}$$

$$E_{\varphi_i} = \cos\theta_i\left(P_{y_i}\cos\varphi_i - P_{x_i}\sin\varphi_i\right) - \eta\left(Q_{y_i}\sin\varphi_i + Q_{x_i}\cos\varphi_i\right) \tag{9.c}$$

where P_x, P_y, Q_x, and Q_y are the so-called spectrum functions defined as

$$P_{x/y} = \iint_S E_{x/y}(x', y')e^{jk(x'\sin\theta\cos\varphi + y'\sin\theta\sin\varphi)}dx'dy' \tag{10.a}$$

$$Q_{x/y} = \iint_S H_{x/y}(x', y')e^{jk(x'\sin\theta\cos\varphi + y'\sin\theta\sin\varphi)}dx'dy'. \tag{10.b}$$

$E_{x/y}$ and $H_{x/y}$ are the tangential components of the transmitted electric and magnetic fields in the subaperture and S is the surface of the radiating subaperture in a $x'y'$ plane.

B. Generalized Intersection Approach

The Intersection Approach (IA) is a well-known optimization method based on alternate projections. The IA searches for the intersection of two sets such that the solution is a field radiated by the antenna geometry and satisfies the desired conditions [25]. One set is defined by all the fields radiated by the antenna ($\mathcal{R}$), whereas the other is defined by the fields that meet the specifications ($\mathcal{M}$). The forward projector $\mathcal{F}$ is classically defined to satisfy (9). Therefore, from a field radiated by the antenna $\boldsymbol{E}_{NF}^{i}$ in the i-th iteration, a projection $\widetilde{\boldsymbol{E}}_{NF}^{i}$ satisfying the specifications is obtained:

$$G_{lwr}(\boldsymbol{r}) \leq |\widetilde{\boldsymbol{E}}_{NF}^{i}(\boldsymbol{r})| \leq G_{upr}(\boldsymbol{r}) \tag{11}$$

where G_{lwr} and G_{upr} are the lower and upper boundaries, respectively. The field $\widetilde{\boldsymbol{E}}_{NF}^{i}$ corresponds to that calculated in the i-th iteration of the IA and $\boldsymbol{r}$ is the point of observation where the field is evaluated.

Then, the backward projector $\mathcal{B}$ retrieves $\widetilde{\boldsymbol{E}}_{NF}^{i}$ to $\mathcal{R}$ trying to obtain the closest radiated field $\boldsymbol{E}_{NF}^{i+1}$ to the desired solution. For this projection, the Intersection Approach in its classical

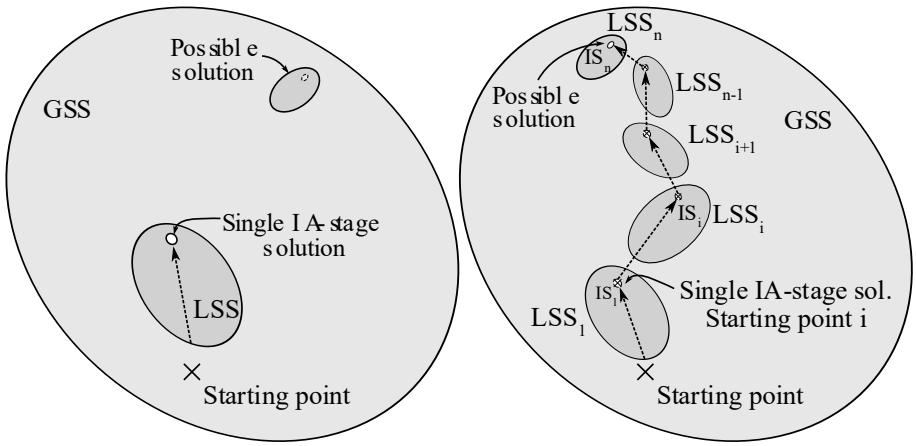

(a) (b)

Fig. 2. Scheme of the displacement of local search space through (b) the proposed Field-to-Mask (F2M) adaptive process compared with (a) a single stage strategy.

implementation and other algorithms based on alternate projections, retrieve the tangential field in the aperture from $\widetilde{\boldsymbol{E}}_{NF}^{i}$ using the FFT [20]. However, this limits the regions where the specifications are established to planes parallel to the antenna aperture, for arbitrary regions the FFT cannot be used.

The alternative used in this work is the gIA, which defines a backward projector based on an optimization algorithm [29]. A well-known problem of optimizers are the local minima reached, which are so-called traps. Two sources of traps may be found in the Intersection Approach. First, the number of degrees of freedom (number of optimizing variables). Second, the non-convexity of the sets. The latter can be overcome by working with the radiated intensity instead of the field itself [16]. Hence, (11) is rewritten as

$$G_{lwr}^2(\boldsymbol{r}) \leq |\widetilde{\boldsymbol{E}}_{NF}(\boldsymbol{r})|^2 \leq G_{upr}^2(\boldsymbol{r}) \tag{12}$$

The overall of the gIA is to define a functional, such as (13) that evaluates the distance between an element of $\mathcal{M}$ and another of $\mathcal{R}$. Then, this functional can be used as a cost function that is minimize by the optimization algorithm selected to implement the backward projector.

$$d = \int_{\boldsymbol{\Omega}} \omega(\boldsymbol{r}) \left((|\widetilde{\boldsymbol{E}}_{NF}(\boldsymbol{r})|^2 - |\boldsymbol{E}_{NF}(\boldsymbol{r})|^2) \right)^2 d\boldsymbol{\Omega} \tag{13}$$

where $\boldsymbol{\Omega}$ is the volume of the Fresnel region wherein the radiated near field is computed, $\boldsymbol{r}$ is an observation point within $\boldsymbol{\Omega}$, and $\omega(\boldsymbol{r})$ is a weighting function. The evaluation of d is done point by point, so that Ω can be discretized into a grid of $N_x \times N_y \times N_z$ points. Therefore (13) can be discretized leading to (12):

$$d = \sum_{i=1}^{N_\Omega} \omega_i(\boldsymbol{r}) (|\widetilde{\boldsymbol{E}}_{NF}(\boldsymbol{r})|^2 - |\boldsymbol{E}_{NF}(\boldsymbol{r})|^2) \, \Delta_{\Omega,\mathrm{i}} \tag{14}$$

where N_Ω is the number of sub-volumes at which the volume is discretized, and Δ_Ω is the sampling used. This function is similar to

$$F(x) = \sum_{i=1}^{M} \left(r_{\mathrm{i}}(x) \right)^2 \tag{15}$$

where $r(x)$ is known as residual and it is discretized in M points.

Then, (14) and (15) are similar, so that the discretized functional d can be used as the cost function of a local optimizer like LMA (Levenberg Marquard Algorithm) [16].

The ideal solution is to reach a point that belongs to both sets simultaneously. Hence, the near field radiated by the metalens fulfils the specifications. If the intersection is not reached, or it is even unreachable, at least to find a radiation pattern whose distance to $\mathcal{M}$ is minimal.

The implementation proposed in this work of a generalized version of IA enables to freely impose conditions in planes with arbitrary shapes and orientations in space overcoming the limitation of the FFT in IA that only permits to impose constrains in planes parallel to the aperture.

III. Multi-Stage Adaptive Field-To-Mask procedure

A. F2M description.

The IA is a powerful technique to shape the copolar component of both radiated far and near fields. However, local search algorithms (as the IA) are strongly affected by the starting point and the desired specifications. In case of very tight requirements, the possible solutions of the synthesis procedure form a very reduced set belonging to the Global Search Space (GSS). If the starting point of the IA is not properly selected, the algorithm can converge to a local minimum belonging to the Local Search Space (*LSS*) without reaching a proper solution, as Fig. 2(a) shows. For complex shaped patterns and tight constraints, the selection of a good starting point could become a very challenging task. Moreover, when dealing with near field other inherent characteristics of electromagnetic waves must be also considered in the templates/masks. For instance, the propagation of electromagnetic waves or complex geometries of the scenario might directly lead to complex patterns. All those effects can imply a hard definition of the templates/mask, and they thus can endanger the convergence to a valid solution.

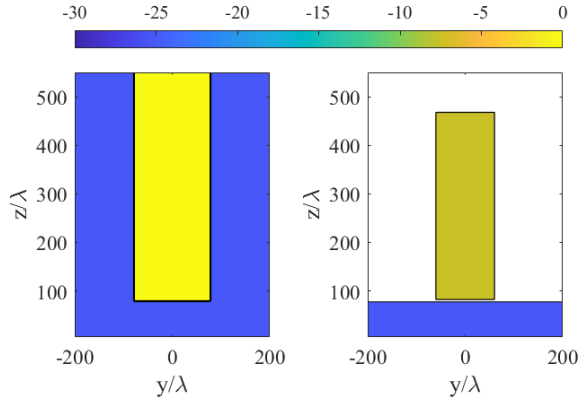

Fig. 3. Mask used in the single IA-stage for widening a Bessel beam. Mask of maximum (left) and mask of minimum values (right) in dB. The white area represents a value lower than −100 dB.

A strategy to improve this convergence is to carry out a concatenated multi-stage synthesis process where the initial templates/masks are related to specifications but laxer than final requirements. Using laxer requirements at the initial stage simplifies the selection of the initial starting point thus, to converge to an initial solution (IS_1) that meets these initial templates. Then, during the following intermediate stages, the templates become tighter as they adaptatively adjust to the final desired specifications. Adjusting the templates at each stage i, the Local Search Space at this stage (LSS_i) will change intending to include a valid solution for the required specifications. The changes in the templates at a given stage will be a function of the required specifications and the achieved intermediate solution (IS_{i-1}) in the previous stage. Therefore, the intermediate solution obtained in the stage $i-1$ can be used as the starting point in the stage i. Fig. 2(b) presents an overall view of this strategy.

The starting point (initial radiated field $\boldsymbol{E}_{NF}^{1}$) and the shaped geometry of the specifications are used to set the first intermediate specifications (in terms of an intermediate mask IM_1). The initial Local Search Space (LSS_1) is defined as the space wherein the algorithm will try to find the first intermediate solution (IS_1). Then, solution IS_1 is used as both starting point of the second stage and to define a second set of intermediate masks (IM_2), defining a new LSS_2 wherein IS_2 is found. Following this process, IM_i, LSS_i, and IS_i will progressively evolve to a final LSS_n, which contains a solution that satisfies the desired specifications.

This strategy highly depends on a proper selection of both starting point and definition of the intermediate specifications at each stage to converge to a proper intermediate solution. Either in a single-stage or multi-stage synthesis, the specifications are typically given in form of templates/masks, and they are defined in terms of the radiated field and certain requirements, such as gain (in the case of far-field specifications), ripple, SLL or shaping while the starting point is commonly given by an analytical approach.

This adaptive definition of the specifications is applied in terms of adaptive templates/masks in each intermediate stage (IM_i). The templates/masks will be defined according to the final specifications (ripple, field distribution, gain, …) and the

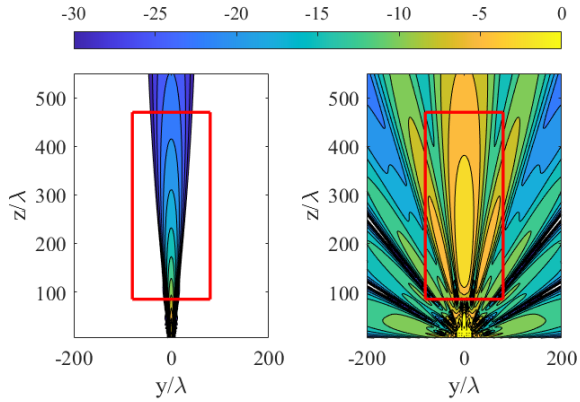

(a) (b)

Fig. 4. Near-field pattern normalized (dB) obtained as (a) starting point (b) after the synthesis using a single IA-stage strategy. The red line is the limit of the area in which the Bessel beam should be widened. The near field pattern is normalized to the maximum within the red limits.

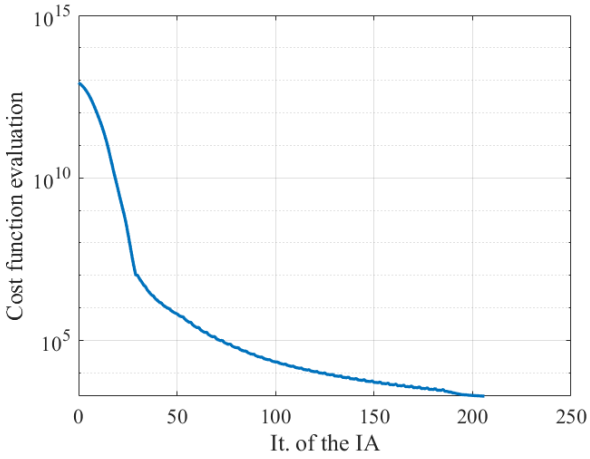

Fig. 5. Evaluation of the convergence of the single IA-stage.

radiated field distribution obtained as a solution in the previous stage $i-1$. After several concatenated stages using as a starting point the solution of the previous stage and progressively adjusting the intermediate specifications/masks according to the field obtained, the different stages will lead the algorithm to a LSS that contains a valid solution, therefore, achieving an output that meets the desired requirements.

B. F2M versus single IA-stage.

This subsection is devoted to detail a F2M procedure compared with a single IA-stage. To do so, we are going to use a metalens comprised of 40×40 elements radiating a Bessel beam. Then, the conventional single IA-stage and the F2M is used to widen the non-diffractive range along the propagation direction, as well as the transversal direction. The focus is placed in the mask definition, the convergence and the near field obtained comparing the two strategies.

In a single IA-stage the mask is specified at the beginning of the synthesis according to the desired requirements. In this case, the aim is to obtain a range with less than 6 dB of field decay within a range from 85λ to 470λ (30 GHz) in the longitudinal direction, and $\pm 80\lambda$ in the transversal direction (see Fig. 3).

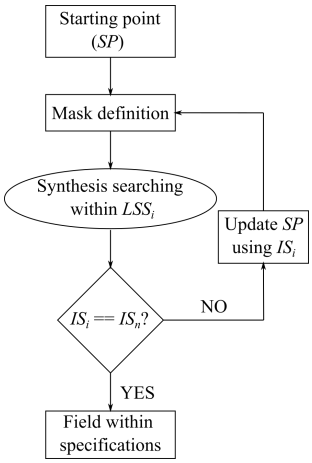

Fig. 6. Flowchart of the synthesis based on a F2M procedure.

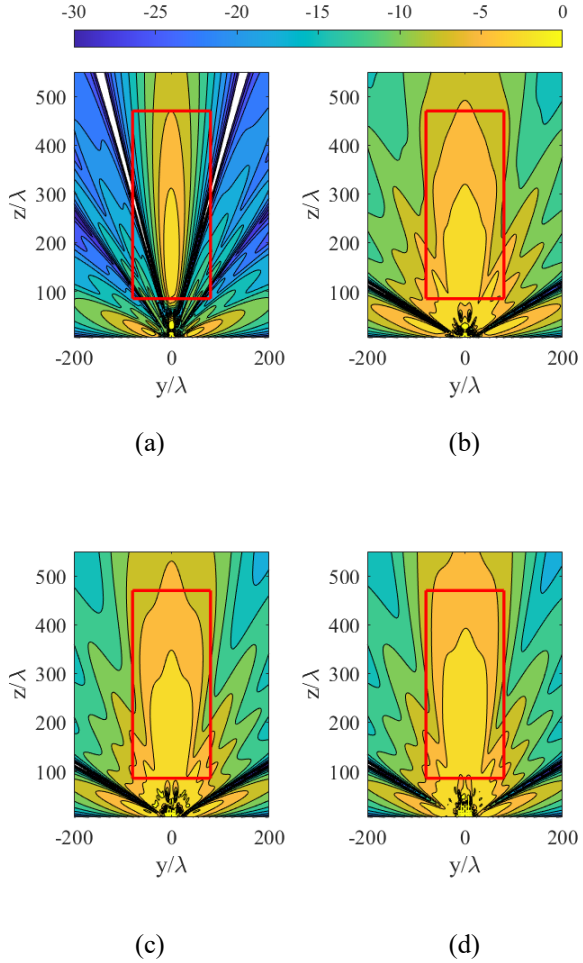

Fig. 7. Normalized near-field pattern (dB) obtained at the different stage of a F2M strategy. The starting point is an analytical Bessel beam (Fig.4(a)). (a) Stage I (b) Stage II (c) Stage III and (d) Stage IV. The red line is the limit of the area in which the beam should be widened. The near field pattern is normalized to the maximum within the red line.

Outside this area the field should be as low as possible, being the maximum acceptable value -25 dB bellow the maximum. The starting point (*SP*) is the near field pattern obtained with the analytical phase distribution is shown in Fig. 4(a). As it was pointed out before, this first synthesis is based on a single IA-stage, therefore the desired solution should be directly obtained from this starting point. The output near field pattern after 204 iterations of the IA is shown in Fig. 4(b). Although the convergence of the algorithm is good as shown in Fig. 5, the reached solution lies within the *LSS* generated by the starting point but does not meet the desired specifications. The obtained near field pattern is widened in the longitudinal cut but not in the transversal direction. Moreover, some of the radiated power is spread in other directions, generating nulls in the desired area.

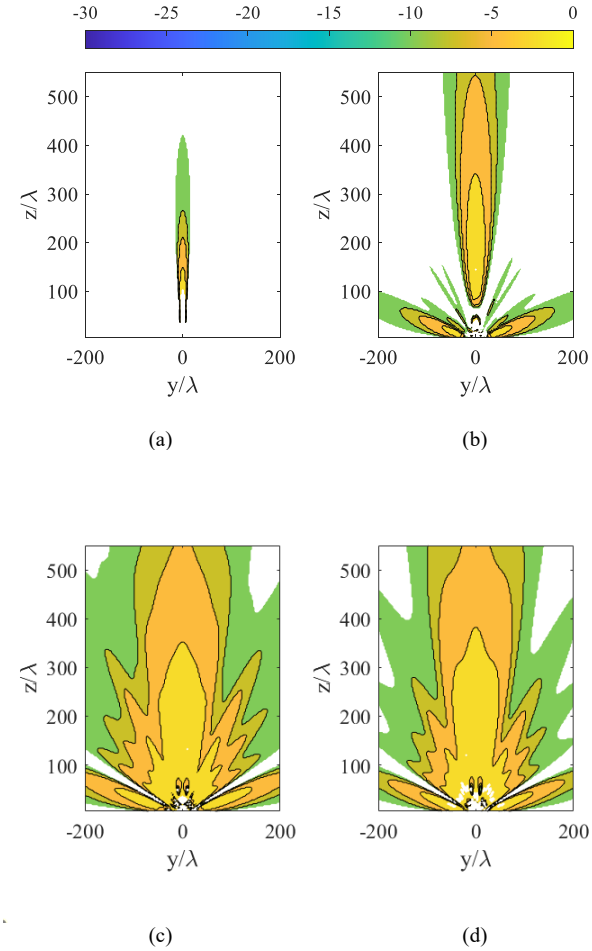

Fig. 8. Mask defined for the F2M synthesis at different stages: (a) Stage I (b) Stage II (c) Stage III and (d) Stage IV. This is the minimum boundary template and is defined in dB.

On the other hand, the same synthesis has been performed using the F2M. According to Fig. 2, the same starting point is used, but several intermediate solutions (IS_i) between it and the desired solution (IS_n) will be searched. This IS_i will be close to the starting point to ensure that they are contained within the LSS_i search space. A flowchart of the F2M applied to synthesis is shown in Fig. 6.

The starting point is the field in Fig. 4(a). From this, the different IS_i shown in Fig. 7 have been obtained. It should be remembered that the IS_i in turn is used as the starting point of the following synthesis and defines the new LSS_{i+1}.

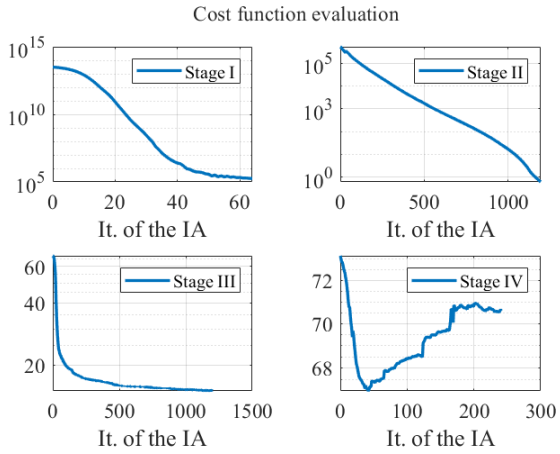

Fig. 9. Evolution of the convergence of the several stages used in the F2M synthesis.

To ensure that the IS_i is contained within the LSS_i and it is achievable, the IS_i is related to the previous starting point (SP_{i-1}) according to the F2M procedure. The definition of the mask will be further detailed in the next Section IV; however, Fig. 8 shows the different masks generated from each IS_{i-1} (that are used as SP_i in each new following stage). In this case, the maximum mask of Fig. 3(a) has been kept for all the stages, modifying only the minimum mask. The mask for the stage i follows a very similar shape to the radiated field of stage $i-1$, ensuring that the solution IS_i is close to the starting point (SP_i), therefore containing IS_i within the LSS_i.Only four stages have been needed to achieve the field of Fig. 7(d). -The convergence of each stage is shown in Fig. 9. In all cases, it has been a good and smooth convergence, reducing the error gradually from the initial starting point (Bessel beam) to the final IS_n (Fig. 7(d)). The final field distribution is very uniform over the desired area, achieving almost a 5 dB difference in field levels over the entire area. In addition, it practically fits the desired rectangular area. Compared to the single IA-stage solution, the field is much more concentrated, with a much smaller field difference and a shape adapted to the desired geometry.

IV. Near-field synthesis using the F2M approach

To better show the performance of an adaptive F2M procedure, we introduce a more challenging example in which this technique is applied. Let us suppose a base station (BS) based on a spatially fed array (a metalens). The BS is integrated into an indoor scenario such as Fig. 10 depicts. The scenario is a building whose shape is a curved corridor that can be modeled as a circular annulus of inner radius ($r_1 = 5$ m) and outer radius ($r_2 = 10$ m). The corridor is divided into 4 areas covered by the BS ANT1-4, being ANT1 and ANT3 identical as well as ANT2 and ANT4. In this work, our interest is focused on the coverage provided by ANT1 since it presents a more complex shape. The coverage is defined in a YZ- plane with the shape of the shadowed area of Fig. 10 at $x = -1.5$ m.

The BS should radiate an almost uniform field distribution within the desired coverage area (shadow area) and minimize the radiation beyond these limits. The aim is to obtain a radiated power density as uniform as possible within the coverage area.

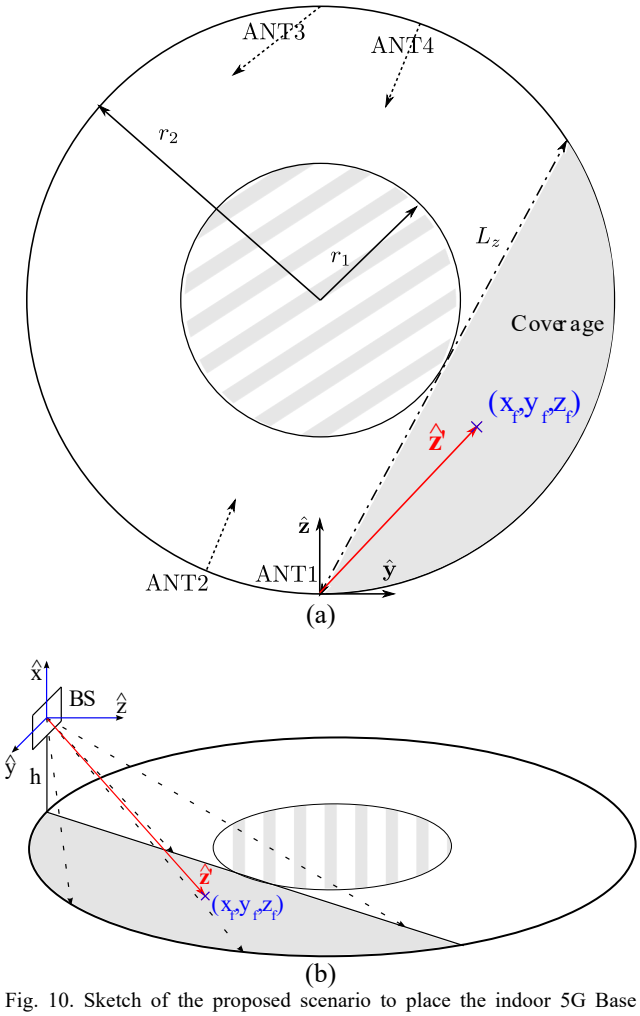

Fig. 10. Sketch of the proposed scenario to place the indoor 5G Base Station and provide a uniform field distribution to enhance the 5G coverage. (a) Top view; (b) Perspective.

Two important challenges are presented in this scenario. First, the geometry of the scenario is not a canonical shape and the L_z (radial distance to the boundary) varies conforming to r_2. Second, the coverage is not defined in a parallel plane to the aperture but a transversal one, and this plane is not a main plane (*xoz* or *yoz*) but an offset one. We might consider that the maximum range in the y-direction might be proportional to the aperture and the projection of the field onto the coverage. However, in the z-direction, it is not clear the maximum range wherein the field can be uniformized. This means that *a priori* it cannot be easily predicted the maximum range in which we can obtain a uniform distribution of the field.

L_z ranges from 0.1 m to 14 m, therefore there is an inherent strong difference in the relative levels of the field due to the propagation of the wave. This effect does not appear when the conditions are imposed in single planes parallel to the antenna aperture or in far-field scenarios. In those cases, the templates/masks are commonly defined using laxer requirements, however, in this scenario a similar approach cannot be easily applied. It is quite difficult to set a proper range throughout the coverage and its variations due to the curved shape of the scenario. Thus, it is quite hard to define a proper template/mask beforehand without endangered the

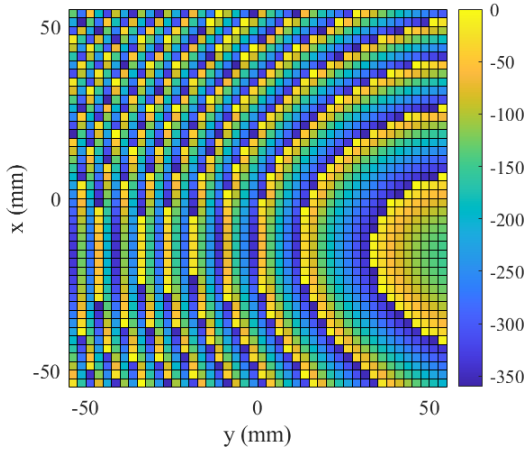

Fig. 11. Phase-shift distribution (deg) on the transmit-array surface for a near-field focused transmit-array.

convergence of the synthesis. The use of the F2M approach might improve the convergence of the algorithm. Besides, the fact that the each searched intermediate solution (IS_i) will be relatively close to the each starting point (IM_i is defined considering the starting point gradually converging the required specification) makes that the election of a starting point is not as critical as in other conventional approaches.

A. Antenna optics and starting point.

The BS antenna is a small metalens antenna of 1936 elements distributed on a regular grid of periodicity of $2.5 \times 2.5\ \text{mm}^2$ in both directions. To achieve a very compact structure the focal distance (F) is 68.5 mm, which provides a F/D of 0.45. The antenna operates at 39 GHz and the feed is a horn antenna of 15 dBi gain and y-polarized (see Fig. 1) with a taper in the amplitude of the incident field of about 20 dB. The $\hat{y}$ component of the near field is the one optimized in the synthesis. According to these antenna optics, most of the coverage is defined within the Fresnel region of the BS. According to Fig. 2 and the process detailed throughout Section III, the starting point is a limiting and critical factor since it establishes the LSS wherein the algorithm searches for the solution. In this case, the starting point is the phase-shift distribution of a near-field focused metalens. To design a metalens that focuses the near field on a point $\boldsymbol{r}_f$, the elements should introduce the phase shift given by

$$\phi_{NFF}(x_l, y_l) = -\frac{2\pi}{\lambda_0}\left(\sqrt{\left(x_f - x_l\right)^2 + \left(y_f - y_l\right)^2 + z_f^2} - d_{f,l}\right) \tag{16}$$

where λ_0 is the wavelength at the operational frequency, $d_{f,l}$ is the distance from the feed to the lth element and $\left(x_f, y_f, z_f\right) = (-1.5, 5.25, 5.5)$ m is the focal point of the metalens. This equation is applied to the geometry defined in this section, obtaining the phase-shift distribution on the metalens shown in Fig. 11.

Fig. 12(a) shows the near field obtained by the phase-shift distribution computed with (16) and the near-field model discussed in Section II. The near-field pattern focuses the field within the desired area and, then the field rapidly decays avoiding radiation in undesired directions, providing a suitable starting point.

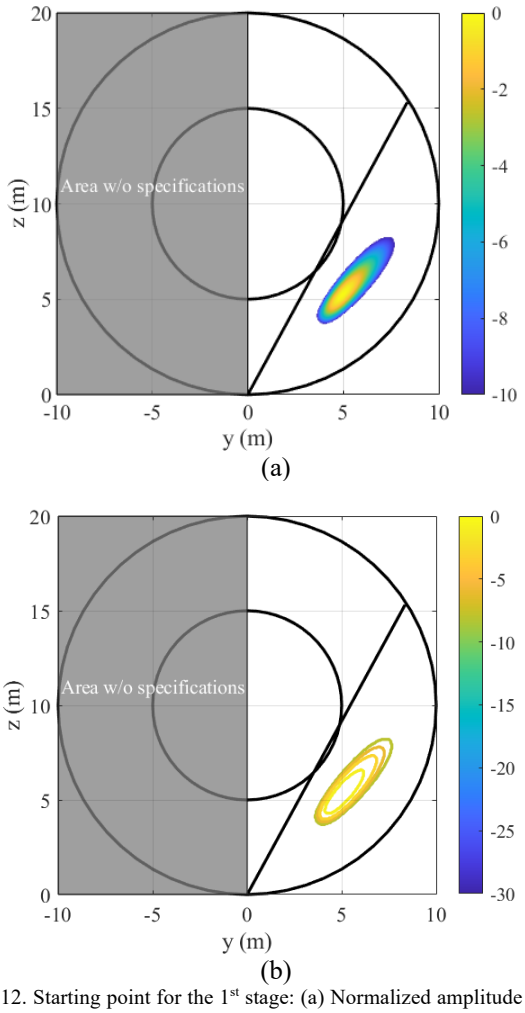

Fig. 12. Starting point for the 1st stage: (a) Normalized amplitude (dB) of the near-field pattern on the footprint coverage. The field is normalized to the focal point of the metalens. (b) Contoured pattern areas used to define the F2M approach considering the starting point of the synthesis (dB). The field is normalized with respect to its maximum.

B. Adaptive F2M procedure

To define an adaptive F2M procedure we take the starting near-field pattern as a reference, see Fig. 12(a). According to the specifications of the coverage, the field must be wide enough to fill the whole coverage. However, the metalens focuses the field on an area around $\boldsymbol{r}_f$, and then, the field rapidly decays in all directions of the longitudinal plane but with different slopes. The field shows a slower decay through the longitudinal direction of the coverage, while the field rapidly decays in the other directions. If the mask is used to modify these different slopes, considering the decay of the field in each direction, according to the final goal, the algorithm is guided to find a solution closer to the starting field pattern than defining arbitrary masks only based on the specifications. Therefore,

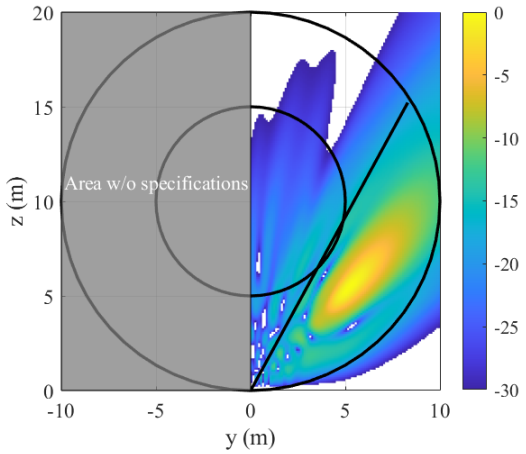

Fig. 13. Normalized amplitude (dB) of the near-field pattern after 7 stages of the process using the proposed adaptive F2M at 39 GHz. The field is normalized with respect to its maximum.

without considering the field pattern and its slopes in each direction.

In Fig. 12(a) the near-field distribution of the starting point is shown superimposed on the footprint of the coverage. Regarding (11), we must set two templates: minimal and maximum boundaries. A feasible approach for an adaptive F2M definition is outlined by the particular implementation of (12) given by

$$G_{lwr}(\boldsymbol{r})\begin{cases} -1 & \text{if } -3 \le |\boldsymbol{E}| \le 0 \\ -3 & \text{if } -6 \le |\boldsymbol{E}| < -3 \\ -6 & \text{if } -8 \le |\boldsymbol{E}| < -6 \\ -8 & \text{if } -10 \le |\boldsymbol{E}| < -8 \\ -10 & \text{if } -12 \le |\boldsymbol{E}| < -10 \\ -\infty & \text{if} |\boldsymbol{E}| < -12 \end{cases} \tag{17.a}$$

$$G_{upr}(\boldsymbol{r}) = \begin{cases} 0 \text{ dB}, & \text{if } |\boldsymbol{E}| \text{ within the coverage} \\ -12 \text{ dB}, & \text{if } |\boldsymbol{E}| \text{ outside the coverage} \end{cases} \tag{17.b}$$

This definition uses as input the field pattern $\boldsymbol{E}$ given by IS_{i-1} and the output is the contoured footprint of the Fig. 12(b). The limit of each contour area is imposed by the field decay, enabling the synthesis to progressively relax and soften the fall of the field. In general, these masks are progressively adapted to the desired solution IS_n, but taking into account the point of previous stage (IS_{i-1}). Applying (17.a), the field decay in stage i should be reduced by $2-3$ dB concerning stage $(i-1)$, so that the field distribution is always made a little more uniform. This concept is totally different from conventional procedures that only take into account the final solution IS_n to define the templates. Note that, the $-\infty$ is implemented by using a low level, e.g., -140 dB, and the mask of maximum level must be used to control parameters such as the SLL or radiation on undesired areas. The mask of maximum level has an important influence to shape the pattern to the desired geometry since it is used to force a strong decay outside of the coverage by imposing a low level of the field (like roll-off factor and SLL in far-field synthesis). This mask of maximum is only set to 0 dB inside the coverage, and it is not redefined during the whole synthesis process. In this case, (17.a) and (17.b) are defined as

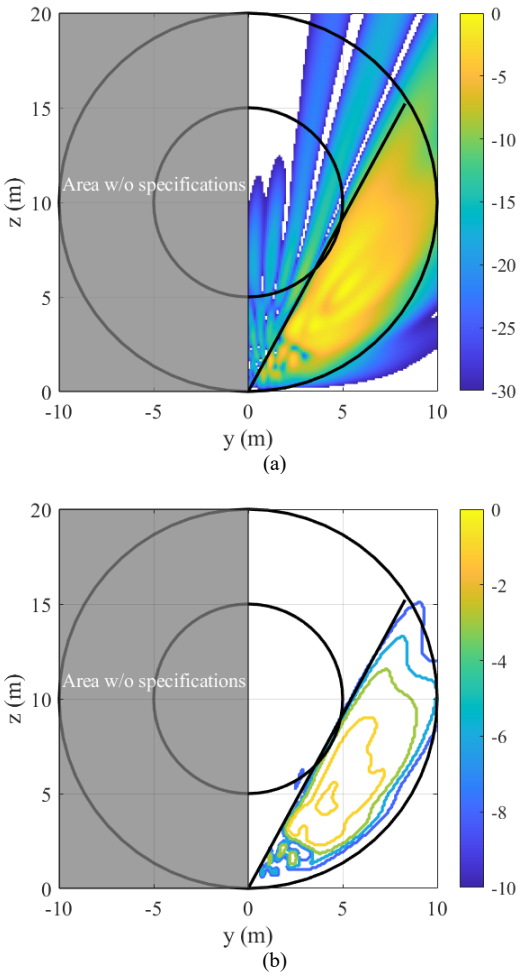

Fig. 14. (a) Normalized amplitude (dB) of the near-field pattern after 14 stages s using the adaptive F2M technique at 39 GHz. (b) Different contour areas of the template used in the next stage. The field is normalized to its maximum.

such because the aim is to uniformize the field distribution. However, if another type of pattern is sought, (17.a) and (17.b) should be suitably redefined.

C. *Synthesis results*

Using the previous starting point and the F2M procedure a phase-only synthesis process is carried out with the generalized Intersection Approach for near field. The synthesis aims to broaden the field distribution to obtain a uniform radiated power density within the coverage of Fig. 10. Fig. 13 shows the near field obtained after 7 stages (synthesis including F2M), starting from the field distribution of Fig. 12 and following (17). To use (17) the field is normalized with respect to its maximum, which allows to modify the slope of the field more gradually than choosing other normalization points. Bearing in mind that F2M is intended to follow the shape of the field itself, the near field pattern obtained in the stage $(i-1)$ (IS_{i-1}) is used to generate the templates of the stage i, as well as starting point ($SP_i = IS_{i-1}$). Although this near-field pattern is still far away from the final goal, it has been widened following the different decays of the field in each direction. Thus, we are guiding the field to the desired goal according to its natural behavior. Once

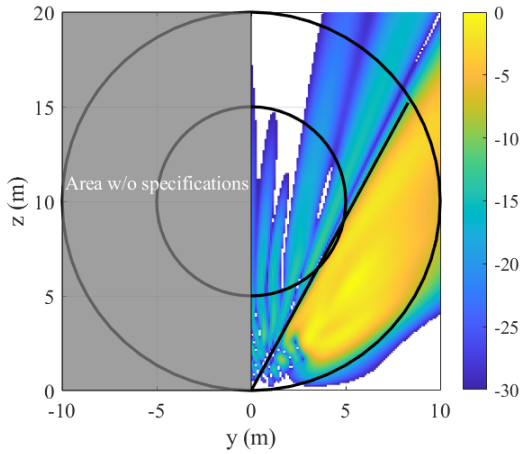

Fig. 15. (a) Normalized amplitude (dB) of the near-field pattern obtained after the entire multistage synthesis process. (b) View of the obtained coverage with a range of only 10 dB. The field is normalized to its maximum.

again, the contour field of the pattern of Fig. 13 and (17) is used to define the next template, and the phase distribution that radiates the pattern of Fig. 13 is the starting point for the next stage.

After 14 stages of the proposed technique, the field pattern of Fig. 14(a) is reached. The near field follows its decay in each direction, and it has been widened considering its pattern shape. This intermediate solution significantly improves the initial point filling an important area of the desired coverage. At this stage, the near-field pattern is close to satisfying the goal but far away from the starting point. In Fig. 14(b) the contoured footprint of the template obtained by the near-field pattern is shown. It is worth noting that the template takes into consideration most of the singularities of the field. For instance, about $(y = 4.3, z = 5)$ m the field presents a local minimum, which value is around $2 - 3$ dB lower than the adjacent points. The F2M technique allows to define masks taking into account the singularities of the field itself. For example, areas where the values are significantly lower than others where the conditions are imposed. In this way, the mask defined using the F2M technique will ask the algorithm for a solution that presents an amplitude with values close to the singularity presented in that

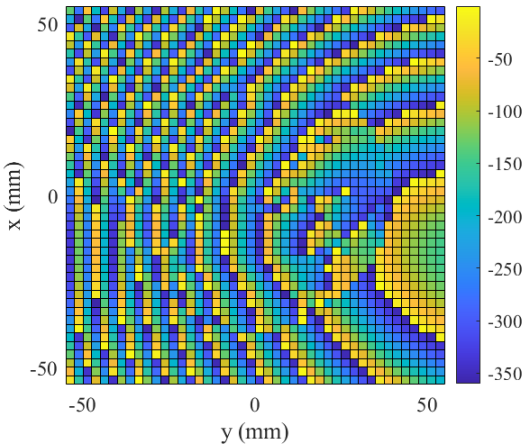

Fig. 16. Phase-shift distribution (deg) on the surface of the metalens after the synthesis process carried out with the generalized Intersection Approach.

area. Thus, the F2M allows to control particular areas of the field, in a progressive manner without requiring abrupt changes as would occur in a classical definition of the masks. Therefore, the algorithm would try to gradually changes the field instead of directly imposing conditions that cannot be reached by the current field. Hence, compromising the convergence.

A total of 27 stages are required to find out a near-field pattern that covers most of the coverage with a smooth field variation. The field pattern is shown in Fig. 15 and the final phase-shift distribution of the elements of the metalens is shown in Fig. 16. This near field presents a very uniform and smooth distribution through the whole desired coverage. Before the synthesis, the difference between the highest and lowest field level is more than 30 dB. After the synthesis this difference is reduced to only 5 dB, resulting in a much more uniform field distribution. This reduction is quite challenging considering that the coverage range is 14 m long. In the closest surrounding area ($z < 3$ m and $y < 2$ m), the smooth coverage is not properly achieved, and a blind area is found. However, this effect may be expected since the starting near-field pattern does not have a significant level in this area (see Fig. 12). Hence, the definition of the adaptive F2M does not impose requirements within this area according to (17). This effect could be reduced by imposing specific requirements in the area to improve the control of the field.

V. Experimental Validation

A. Metalens design and implementation

Once the final phase-shift distribution on the metalens surface is obtained, the elements are designed. The unit cell is a perforated slab of a single dielectric block compatible with a 3D printing solution. In this case, the material is Polylactic Acid, (PLA, $\epsilon_r = 2.98$, $\tan\delta = 0.0148$) and the manufacturing technique is Fused Deposition Modeling (FDM). The unit cell is sketched in Fig. 17. The dimensions of the main square prism are $0.32\lambda_0 \times 0.32\lambda_0 \times 2.34\lambda_0$ at 39 GHz. The embedded prism has a variable dimension from 1 mm to 2.3 mm and a constant height of $2.34\lambda_0$. The working principle is based on a variation of the density of the material

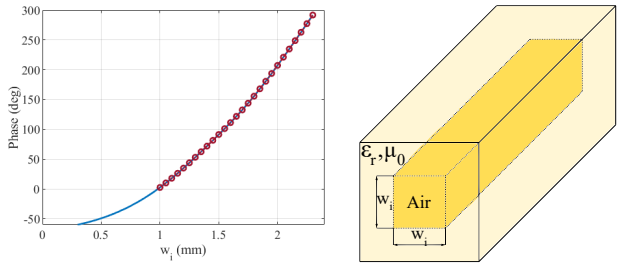

(a) (b)

Fig. 17. Dielectric-only unit cell used to design the metalens: (a) phase delay (deg) of the (b) proposed unit cell according to w_i.

so that a phase shift variation is produced [30]. Hence, the phase

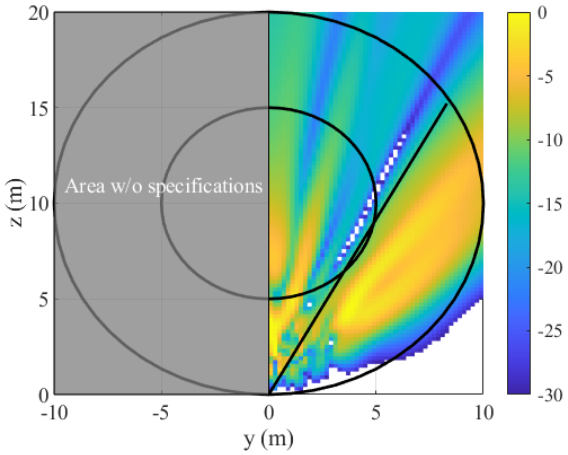

Fig. 18. Near field (dB) obtained through a full-wave simulation considering the dielectric-only transmitarray at 39 GHz. The field is normalized with respect to its maximum.

response of the unit cell depends on the variation of w_i.

The design of the metalens is carried out element-by-element finding the unit cell that provides a phase-shift similar to the synthesis output. Besides, the criteria are minimizing the phase error while the transmission loss is better than -1.2 dB. This criterion is imposed because of the high losses of the PLA, so that it is a trade-off between the phase delay range and the losses. The output of this process is a dielectric slab layout whose air gap insertions introduce the required phase shift. The analysis and design of the unit cells assumes local periodicity, which is the standard assumption in periodic and quasi-periodic structures [15]. However, the phase-shift distribution presents phase jumps and areas with large phase variation due to the synthesis process. This effect reduces the accuracy of analysis technique since the local periodicity approach is not so realistic, and therefore the radiated field thus might be affected. To properly evaluate the real performance of the antenna, considering the effect of the deep phase transitions (phase jumps plus areas of strong fluctuation) the entire antenna is full wave simulated with CST Microwave Studio [31]. In Fig. 18 the full-wave result is given for the copolar component (electric field polarized according to $\hat{y}$) of the near field in the coverage plane at 39 GHz. The near field is evaluated in a symmetric area from $y \in [0,10]$m and $z \in [0,20]$ m, which is the area included in the synthesis. This result highly agrees with the near-field pattern obtained after the synthesis, resulting in an almost

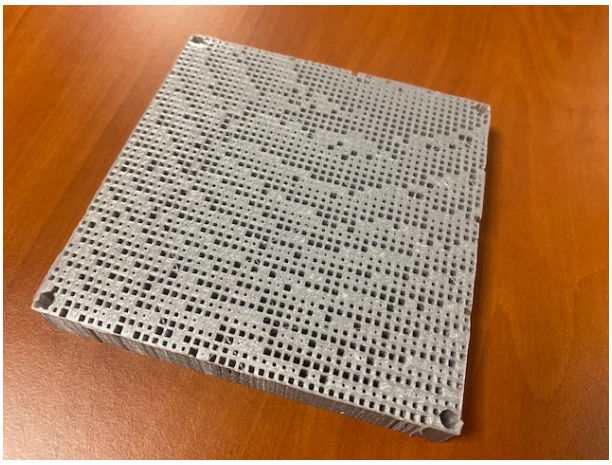

Fig. 19. Prototype of the manufactured metalens.

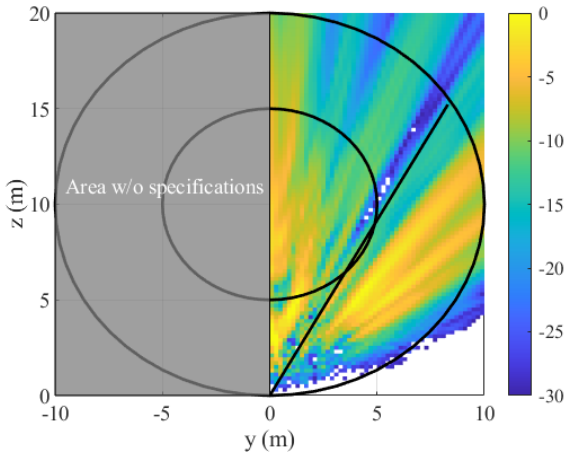

Fig. 20. Near field (dB) radiated by the prototype (measurements) through the coverage at 39 GHz. The field is normalized with respect to its maximum.

uniform field distribution through an extensive coverage area. Besides, the proposed dielectric-only metalens shows a good trade-off between the radiation performance and the complexity of the antenna design.

B. Measurements

The metalens designed in the previous section has been manufactured using the 3D printer Ultimaker 3, resulting in the prototype shown in Fig. 19. The prototype is measured in the planar acquisition range at the Universidad de Oviedo. Due to the vast extension of the coverage and the physical limitations of the facilities, the resulting coverage has been obtained using a two-step procedure. First, the electric field radiated by the metalens is evaluated in a plane close to the antenna, particularly at 100 mm, and parallel to the aperture. The field is measured within a regular grid of 250×250 mm^2 sampling at 2.5 mm (0.32λ@39 GHz). This grid ensures that most of the electric power is captured. To measure the electric field the metalens is placed in a PLA structure that also holds the horn antenna of 15 dBi used as feed (Flann 22240-15). The probe is an open-ended waveguide at the K_a-band oriented according to the polarization of the electric field. Second, the near field at

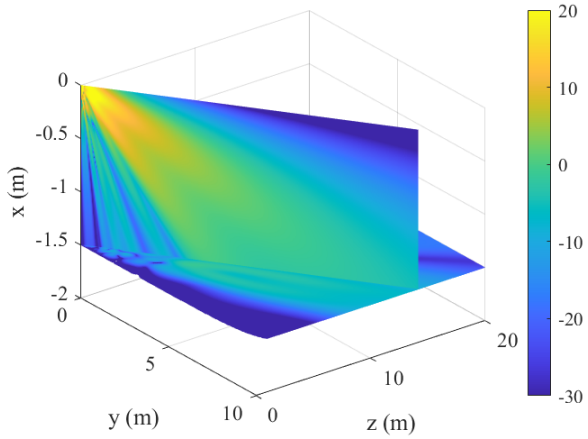

(a)

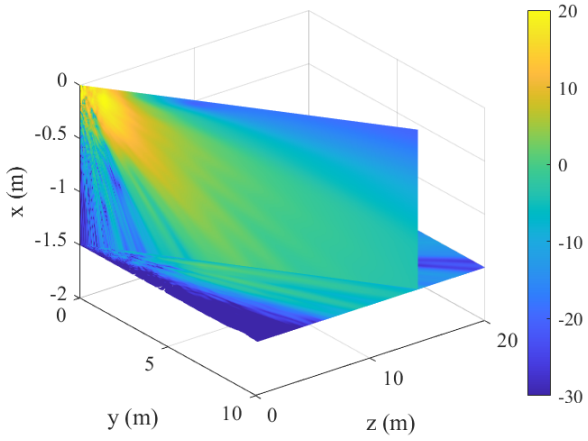

(b)

Fig. 21. Comparison of the near-field pattern (dB) obtained through (a) full-wave simulations and (b) measuring the prototype at the coverage plane and a middle plane of the coverage at 39 GHz.The field is normalized to the level at the focus point of the metalens.

the coverage plane is obtained with a NF-NF transformation with GRASP [32] based on a Spherical Wave Expansion (SWE). The measurements have been carried out from 38 to 40 GHz.

The resulting near field through the coverage plane is shown in Fig. 20. The near-field pattern presents a mostly uniform field distribution at the desired area, as the synthesis and full-wave simulations show before. In the area of interest, the near-field pattern presents similar levels and shapes. Both near-field patterns are quite similar in terms of the relative levels of the electric field along the coverage, as well as the shape of the coverage. The proposed antenna obtains a smooth relative level difference in the radiated field, highlighting that the coverage goes up to more than 14 m and it is defined through a plane transversal to the aperture. Besides, the shape is adjusted to a tangential plane of the inner circle and shaped according to the curve described by the external circle. The difference between both the full-wave simulations and the measurements might be associated with the manufacturing process. The prototype is manufactured using FDM, which is a very affordable technique at the cost of decreasing the accuracy compared with other techniques. Moreover, some walls between adjacent cells

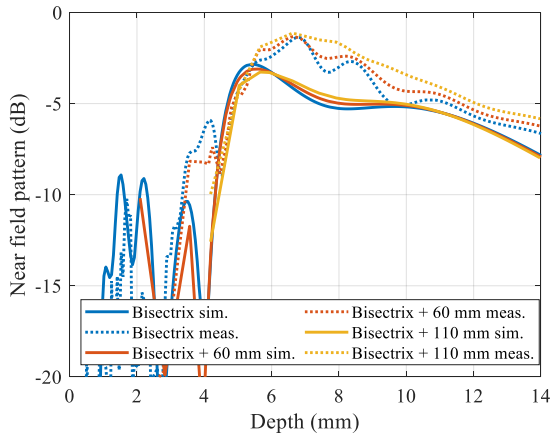

Fig. 22. Several cuts of the near field pattern (dB) of Fig. 21 at 39 GHz. The field is normalized to the level at the focus point of the metalens.

TABLE I – In-band performance of the measured coverage within a 2 GHz bandwidth.

Freq. (GHz)	*Max E field Intensity (dB)* *Normalized to central frequency*	*Ripple (dB)*
38	5.93	16.67
38.5	5.81	18.18
39	0.69	16.18
39.5	3.60	18.17

require an extremely low thickness, i.e., less than 0.1mm. However, the measurements show a high agreement with the full-wave and synthesis results, considering the complexity of the proposed scenario.

Fig. 21 shows the horizontal plane of the coverage together with a transversal plane defined in the vertical middle plane of the coverage. This plane shows that the radiated power is focused on the coverage area, and it is not radiated into undesired directions, which is a common issue when dealing with near-field synthesis. Full-wave simulations are compared with the measurements, obtaining a high agreement between both. Moreover, Fig. 22 shows several cuts of both figures to have a detailed comparison of the results.

In Table I the in-band performance of the antenna is shown for a bandwidth of 2 GHz. In particular, the peak-to-peak ripple in the coverage and the maximum electric field intensity have been evaluated. These values are obtained for the uniform zone resulting in the coverage plane. Both results show that the coverage is stable at least in 2 GHz bandwidth, providing a very uniform coverage. This fact is mainly due to the use of dielectric-only elements, which inherently provide better bandwidths than resonant elements.

VI. Conclusion

A novel technique to address the synthesis of metalens antennas with tight requirements in complex scenarios has been presented in this work. The technique is based on a multi-stage procedure where the local search space is moved progressively from the starting point to the final requirements point. In the intermediate stages the templates for the synthesis process are defined based on the field radiated by the antenna in the last iteration of the previous stage, in a field-to-mask (F2M). This

procedure has been implemented with the generalized Intersection Approach algorithm and a near-field model of the metalens that are also introduced, which permits the synthesis in arbitrary spatial domains. Moreover, the F2M procedure can be applied in any local-search optimizer.

The technique is applied to the synthesis of a smooth coverage in a long and curved corridor for 5G indoor efficient deployment. The metalens is placed at the top of a wall and provides a low-ripple coverage at 39 GHz in more than 10 meter range, defined on a plane transversal to the antenna aperture and parallel to the floor. The application case demonstrates the performance of the proposed technique to obtain long and smooth coverages.

Finally, the result of the synthesis process is used to design a dielectric-only metalens antenna. It is manufactured with additive manufacturing process and the antenna is measured in close near field using a planar acquisition range in anechoic environment. Then, the near field to near field transformation is used to evaluate the coverage performance in the defined scenario. The comparison of synthesis results, full-wave simulations and measurements demonstrates the capability of the proposed technique to provide smooth coverage in complex indoor scenarios for the efficient deployment of upcoming mobile networks in mm-wave bands.

ACKNOWLEDGMENT

The authors would like to thank the collaboration from Mr. Mateo García-Valles throughout the design of the antenna.

REFERENCES

[1] H. Chou, C. Yu, K. Wang and P. Nepa, "A Simple Design of Patch Antenna Array With an Optimized Field Distribution in the Near-Zone for RFID Applications," in *IEEE Antennas and Wireless Propagation Letters*, vol. 13, pp. 257-260, 2014.

[2] P. Zhang, L. Li, X. Zhang, H. Liu and Y. Shi, "Design, Measurement and Analysis of Near-Field Focusing Reflective Metasurface for Dual-Polarization and Multi-Focus Wireless Power Transfer," in *IEEE Access*, vol. 7, pp. 110387-110399, 2019.

[3] L. Dussopt, K. Medrar and L. Marnat, "Millimeter-Wave Gaussian-Beam Transmitarray Antennas for Quasi-Optical S-Parameter Characterization," in *IEEE Transactions on Antennas and Propagation*, vol. 68, no. 2, pp. 850-858, Feb. 2020.

[4] 3rd Generation Partnership Project, 3GPP Release 16 Description, 2020.

[5] T. S. Rappaport, Y. Xing, G. R. MacCartney, A. F. Molisch, E. Mellios and J. Zhang, "Overview of Millimeter Wave Communications for Fifth-Generation (5G) Wireless Networks-With a Focus on Propagation Models," in *IEEE Trans. Antennas Propag.*, vol. 65, no. 12, pp. 6213-6230, Dec. 2017.

[6] W. Hong *et al.*, "The Role of Millimeter-Wave Technologies in 5G/6G Wireless Communications," in *IEEE Journal of Microwave*, vol. 1, no. 1, pp. 101-122, Jan. 2021.

[7] M. Shafi *et al*., "Microwave vs. Millimeter-Wave Propagation Channels : Key Differences and Impact on 5G Cellular Systems," in *IEEE Commun. Mag.*, vol. 56, no. 12, pp. 14-20, Dec. 2018.

[8] K. Zheng, D. Wang, Y. Han, X. Zhao and D. Wang, "Performance and Measurement Analysis of a Commercial 5G Millimeter-Wave Network," in *IEEE Access*, vol. 8, pp. 163996-164011, 2020.

[9] J. Huang, C. Wang, R. Feng, J. Sun, W. Zhang and Y. Yang, "Multi-Frequency mmWave Massive MIMO Channel Measurements and Characterization for 5G Wireless Communications Systems," in *IEEE Journal on Selected Areas in Communications*, vol. 35, pp. 1591-1605, Apr. 2017.

[10] E. L. Bengtsson, F. Rusek, S. Malkowsky, F. Tufvesson, P. C. Karlsson and O. Edfors, "A Simulations Framework for Multiple-Antenna Terminals in 5G Massive MIMO Systems," in *IEEE Journal on Selected Areas in Communications*, vol. 35, pp. 1591-1605, Apr. 2017.

[11] Á. F. Vaquero, D. R. Prado, M. Arrebola and M. R. Pino, "Reflectarray antenas for 5-G indoor coverage," in *Proc. 2019 13th Eur. Conf. Antennas Propag.*, Krakow, Poland, 2019, pp. 1-4.

[12] A. Mudonhi, M. Lotti, A. Clemente, R. D'Errico and C. Oestges, "RIS-enabled mmWave Channel Sounding Based on Electronically Reconfigurable Transmitarrays," *2021 15th European Conference on Antennas and Propagation (EuCAP)*, 2021, pp. 1-5.

[13] Z. -Y Zhang, G. Fu, W. -J. Wu, J. Lei and S. -X. Gong, "A Wideband Dual-Sleeve Monopole Antenna for Indoor Base Station Application," in *IEEE Antennas and Wireless Propagation Letters*, vol. 10, pp. 45-48, 2011.

[14] K. L. Lau and K. M. Luk, "A wide-band monopolar wire-patch antenna for indoor base station applications," in *IEEE Antennas and Wireless Propagation Letters*, vol. 4, pp. 155-157, 2005.

[15] J. Huang and J. A. Encinar, *Reflectarray antennas*, IEEE Press/Wiley, Piscataway, NJ/New York, 2008.

[16] D. R. Prado *et al.*, "Efficient Crosspolar Optimization of Shaped-Beam Dual-Polarized Reflectarrays Using Full-Wave Analysis for the Antenna Element Characterization," in *IEEE Transactions on Antennas and Propagation*, vol. 65, no. 2, pp. 623-635, Feb. 2017.

[17] J. A. Encinar *et al.*, "Dual-Polarization Dual-Coverage Reflectarray for Space Applications," in *IEEE Trans. Antennas and Propag.*, vol. 54, no. 10, pp. 2827-2837, Oct. 2006.

[18] C. C. Cruz, C. A. Fernandes, S. A. Matos and J. R. Costa, "Synthesis of Shaped-Beam Radiation Patterns at Millimeter-Waves Using Transmit Arrays," in *IEEE Transactions on Antennas and Propagation*, vol. 66, no. 8, pp. 4017-4024, Aug. 2018.

[19] S. Yu, N. Kou, Z. Ding and Z. Zhang, "Design of Dual-Polarized Reflectarray for Near-Field Shaped Focusing," in *IEEE Antennas and Wireless Propagation Letters*, vol. 20, no. 5, pp. 803-807, May 2021.

[20] Loredo, G. León and E. G. Plaza, "A fast approach to near-field synthesis of transmitarrays," in *IEEE Antenna and Wireless Propagation Letters*, vol. 20, no. 5, pp. 648-652, 2021.

[21] Á. F. Vaquero, M. Arrebola, M. R. Pino, R. Florencio and J. A. Encinar, "Demonstration of a Reflectarray With Near-Field Amplitude and Phase Constraints as Compact Antenna Test Range Probe for 5G New Radio Devices," in *IEEE Transactions on Antennas and Propagation*, vol. 69, no. 5, pp. 2715-2726.

[22] D. R. Prado, Á. F. Vaquero, M. Arrebola, M. R. Pino and F. Las-Heras, "Acceleration of Gradient-Based Algorithm for Array Antenna Synthesis with Far-field or Near-field Constraints," in *IEEE Transactions on Antennas and Propagation*, vol. 66, no. 10, pp. 5239-5248, Oct. 2018.

[23] D. R. Prado, M. Arrebola, M. R. Pino and G. Goussetis, "Contoured-Beam Dual-Band Dual-Linear Reflectarray Design Using a Multiobjective Multistage Optimization," in *IEEE Transactions on Antennas and Propagation*, vol. 68, no. 11, pp. 7682-7687, Nov. 2020.

[24] D. R. Prado and M. Arrebola, "Effective XPD and XPI Optimization in Reflectarrays for Satellite Mission," in *IEEE Antennas and Wireless Propagation Letters*, vol. 17, no. 10, pp. 1856-1860, Oct. 2018.
J. Sherman, "Properties of focused apertures in the Fresnel region," in *IRE Transactions on Antennas and Propagation*, vol. 10, no. 4, pp. 399-408, July 1962.

[25] Á. F. Vaquero, M. R. Pino and M. Arrebola, "Near-field synthesis of spatially-fed arrays for uniform field distribution in complex areas," *2022 16th European Conference on Antennas and Propagation (EuCAP)*, 2022, pp. 1-5.

[26] O. M. Bucci, G. Franceschetti, G. Mazzarella and G. Panariello, "Intersection approach to array pattern synthesis," in *IEE Proc. Microw. Antennas Propag.*, vol. 137, no. 6, pp. 349-357.

[27] C. Tienda, M. Arrebola, J. A. Encinar and G. Toso, "Analysis of a dual-reflectarray antenna," in *IET Microwaves, Antennas & Propagation*, vol. 5, no. 13, pp. 1636-1645, Oct. 2011.

[28] C. A. Balanis, *Antenna theory: analysis and design*. Wiley-Interscience, 2005.

[29] O. M. Bucci, G. D'Elia, G. Mazzarella, and G. Paraniello, "Antenna pattern synthesis: A new general approach," in *Proc. IEEE*, vol. 82, no. 3, pp. 358-371, Mar. 1994.

[30] J. Teixeira, S. A. Matos, J. R. Costa, J. M. Felício and C. A. Fernandes, "Assessing different monoblock dielectric implementations of a low profile beam steering Transmitarray for 3D printing," *2022 Microwave Mediterranean Sysmposium (MMS)*, 2022, pp. 1-3.

[31] *CST*, Compute Simulation Technology AG, Darmstadt, Germany.

[32] *GRASP V10*, TICRA, Copenhagen, Denmark, 2016.

Álvaro F. Vaquero (Member, IEEE) was born in Salinas, Spain, in 1990. He received the B.Sc., M.Sc., and PhD degrees in telecommunications engineering from the Universidad de Oviedo, Gijón, Spain, in 2015, 2017, and 2021, respectively.

From 2016 to 2021, he was a Research Assistant with the Signal Theory and Communications Area, University of Oviedo. He was a Visiting Researcher at the Antennas and Propagation Group, Instituto de Telecomuncações, Lisbon, Portugal in 2017 and 2021. In December 2021, he joined the Department of Signals, Systems, and Radiocommunications, Group of Applied Electromagnetics, Universidad Politécnica de Madrid, Spain, as a post-Doc Researcher involved in the development of Reflective Intelligent Surfaces (RIS) for 5G/6G networks. He moved back to the University of Oviedo in 2022. In 2023 he was a recipient of a Post-doctoral Fellowship financed by the Spanish Government. He is currently a Research Fellow with the Antennas and Propagation Group, Instituto de Telecomunicações, Lisbon, Portugal, and University of Oviedo. He has authored more than 40 peer-reviewed journals and conference papers. His current research interest includes the development of efficient techniques for the analysis and optimization of spatially fed arrays, especially reflectarray, transmitarray and metasurfaces for near- and far-field applications, the design of Reconfigurable Intelligent Surfaces (RIS), and the design of additive manufacturing antennas in mm-wave frequencies.

Dr. Vaquero has also received several awards, such as the 2021 National Award for the Best Ph.D. Thesis on telecommunication engineering for 5G Innovation for Sustainable Connectivity. He was a co-recipient of the Best Conference Paper Award (Third Prize) in the IEEE International Workshop on Antennas Technology (iWAT) and coauthored two papers shortlisted for the Best Paper Award Competition in Antenna Theory and Design at the 17th European Conference on Antennas and Propagation in 2023.

Marcos R. Pino received the M.Sc. and Ph.D. degrees in telecommunication engineering from the University of Vigo, Spain, in 1997 and 2000, respectively.

In 1998, he was a Visiting Scholar with the ElectroScience Laboratory, The Ohio State University, Columbus, OH, USA. From 2000 to 2001, he was an Assistant Professor with the University of Vigo. Since 2001, he has been with the Electrical Engineering Department, University of Oviedo at Gijón, Spain, where he is currently Full Professor, teaching courses on communication systems and antenna design. From 2017 to 2019, he has spent several months as Visiting Fellow with the Department of Information Engineering, University of Pisa, Italy, collaborating in near-field UHF-RFID applications.

His current research interests include antenna design optimized for both near-field and far-field applications, antenna measurement techniques, and efficient computational techniques applied to EM problems.

Manuel Arrebola (Senior Member, IEEE) was born in Lucena, Spain. He received the M.Sc. degree in telecommunication engineering from the University of Málaga, Málaga, Spain, in 2002, and the Ph.D. degree from the Technical University of Madrid (UPM), Madrid, Spain, in 2008.

From 2003 to 2007, he was a Research Assistant with the Department of Electromagnetism and Circuit Theory, UPM. He was a Visiting Researcher with the Department of Microwave Techniques, Universität Ulm, Ulm, Germany. In 2007, he joined the Department of Electrical Engineering, University of Oviedo at Gijón, Spain, where he is currently an Associate Professor with the Signal Theory and Communications Group. In 2009, he was with the European Space Research and Technology Centre, European Space Agency, Noordwijk, The Netherlands, as a Visiting Researcher. He has been a Visiting Professor with several institutions, such as the Edward S. Rogers Sr. Department of Electrical and Computer Engineering, University of Toronto, Toronto, ON, Canada, in 2018; the Institute of Sensors, Signals and Systems, Heriot-Watt University, Edinburgh, U.K, in 2019; and the Antennas and Propagation Group, Instituto de Telecomuncações, Lisbon, Portugal, in 2023. He has authored and co-authored more than 200 peer-reviewed journals and conference papers. His current research interests include the application of innovative manufacturing techniques in mm and submm-wave antenna design, and the development of efficient analysis, design, and optimization techniques of spatial fed arrays, including reflectarrays and transmitarrays, and periodic structures for near- and far-field applications.

Dr. Arrebola was a co-recipient of the 2007 Sergei A. Schelkunoff Transactions Prize Paper Award from the IEEE Antennas and Propagation Society. He has also received the 2008 Outstanding Ph.D. Thesis Award from UPM and the 2009 National Award for the Best Ph.D. Thesis on Telecommunication Networks and Services. Since 2022, he has been an Associate Editor of the IEEE TRANSACTIONS ON ANTENNAS AND PROPAGATION.